Phytochemistry 200 (2022) 113225

Contents lists available at ScienceDirect

Phytochemistry

journal homepage: www.elsevier.com/locate/phytochem

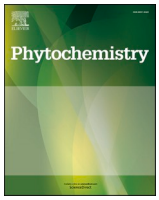

# Marginaols G–M, anti-inflammatory isopimarane diterpenoids, from the rhizomes of *Kaempferia marginata*

Ratchanaporn Chokchaisiri [a,*], Teerawut Thothaisong [b], Warangkana Chunglok [c], Wanatsanan Chulrik [c], Bunlawee Yotnoi [a], Suwadee Chokchaisiri [d], Lucksagoon Ganranoo [a], Sarot Cheenpracha [a], Chutamas Thepmalee [e], Apichart Suksamrarn [b]

[a] Department of Chemistry, School of Science, University of Phayao, Phayao, 56000, Thailand
[b] Department of Chemistry and Center of Excellence for Innovation in Chemistry, Faculty of Science, Ramkhamhaeng University, Bangkok, 10240, Thailand
[c] School of Allied Health Sciences, Walailak University, Nakhon Si Thammarat, 80161, Thailand
[d] College of Allied Health Sciences, Suan Sunandha Rajabhat University, Samut Songkhram, 75000, Thailand
[e] Division of Biochemistry, School of Medical Sciences, University of Phayao, Phayao, 56000, Thailand

ARTICLE INFO

*Keywords:*
Kaempferia marginata
Zingiberaceae
Isopimarane diterpenes
Marginaols
Anti-inflammatory activity

ABSTRACT

Marginaols G–M, a series of undescribed isopimarane diterpenoids, together with four known analogs were isolated from the rhizomes of *Kaempferia marginata*. The structures of these isolated compounds were characterized using high-resolution mass spectrometry and extensive 1D- and 2D-nuclear magnetic resonance (NMR) analyses. In addition, the absolute configurations of marginaol G and H were determined by X-ray crystallographic analysis and comparison with the literature values. When compared to the standard drug dexamethasone ($IC_{50}$ 4.7 $\mu$M), marginaol G, H, and 6$\beta$-acetoxysandaracopimaradien-1$\alpha$,9$\alpha$-diol had an intriguing anti-inflammatory effect on NO inhibition in lipopolysaccharide (LPS)-stimulated RAW264.7 macrophages, with $IC_{50}$ values ranging from 4.5 to 7.3 $\mu$M and being less cytotoxic to the cells. The anti-inflammatory action of these isopimarane diterpenoids from *K. marginata* supports the use of Thai traditional medicine for inflammation treatment.

## 1. Introduction

Inflammation is an immunological reaction to a foreign substance that helps in the restoration of tissue integrity and the maintenance of host homeostasis (Diaz-Jimenez et al., 2021). Macrophages are innate immune cells that, when uncontrolled, can contribute to the pathogenesis of a variety of inflammatory diseases (Ross et al., 2021). The balance of proinflammatory and anti-inflammatory functions in macrophages is among the most important regulators for maintaining cell and tissue homeostasis (Hu et al., 2021). In the presence of inflammatory stimuli, the catalytic activity of inducible nitric oxide synthase produces a significant amount of nitric oxide (NO) and excessive NO generation by macrophages can have detrimental implications (Obaid et al., 2018). As a result, inhibiting macrophage NO generation provides a significant therapeutic benefit in inflammatory disorders. Natural product-based therapeutics for inflammatory diseases have emerged as promising treatment alternatives. Several natural product-based treatments for inflammatory disorders have been investigated in preclinical and clinical research, including curcumin (Fallahi et al., 2021), kaempferol (Devi et al., 2015), epigallocatechin-3-gallate (EGCG) (Seong et al., 2016), resveratrol (Moussa et al., 2017), tetrandrine (He et al., 2011), artemisinin (Efferth and Oesch, 2021), and andrographolide (Tan et al., 2017). The anti-inflammatory characteristics of these compounds support the medicinal use of plants in traditional treatments.

*Kaempferia marginata* Carey ex Roscoe (Zingiberaceae), also known as "Proa pa" in Thai, is a native of Thailand. The rhizome of *K. marginata* has long been used in indigenous medicine to treat allergy symptoms, fever, and swollen legs. Numerous diterpenoids with antiplasmodial, antituberculous, antifungal (Thongnest et al., 2005), anti-allergic (Madaka and Tewtrakul, 2011), and anti-inflammatory activities (Kaewkroek et al., 2013; Chokchaisiri et al., 2020; Do et al., 2022) have been discovered. Recently, we reported the isolation of isopimarane diterpenoids from the rhizomes of *K. marginata* collected from Phana district, Amnat Charoen Province, as well as their anti-inflammatory

* Corresponding author.
*E-mail addresses:* rchokchaisiri@gmail.com, ratchanaporn.ch@up.ac.th (R. Chokchaisiri).

https://doi.org/10.1016/j.phytochem.2022.113225
Received 1 January 2022; Received in revised form 1 May 2022; Accepted 2 May 2022
Available online 7 May 2022

potential (Chokchaisiri et al., 2020). Preliminary analysis of the chemical constituents of this plant species rhizome collected in Phutthaisong district, Buri Ram province (Thailand) revealed that the isopimarane diterpenoid constituents, especially the minor components, differ from previous report findings. To complete the chemical characterization of this plant and to continue the investigation of anti-inflammatory agents derived from medicinal plants, seven undescribed isopimarane diterpenoids, marginaols G–M (**1**–**7**) and four previously described compounds (**8**–**11**), as well as their inhibitory activities on LPS-induced NO production, were isolated and identified from the rhizomes of this plant species.

## 2. Results and discussion

Investigation of the rhizomes of *K. marginata* resulted in the isolation of 11 isopimarane diterpenoids, seven of which are undescribed isopimarane, marginaols G–M (**1**–**7**) (Fig. 1). The known analogs (Fig. S1, Supporting Information) were identified as 1α,14α-dihydroxyisopimara-8 (9),15-diene (**8**) (Tungcharoen et al., 2020), kaempulchraol K (**9**) (Win et al., 2015), 6*β*-acetoxysandaracopimaradien-1α,9α-diol (**10**) (Prawat et al., 1993) and 1α,11α-dihydroxy pimara-8 (14),15-diene (**11**) (Chokchaisiri et al., 2021) by comparison with the literature.

Compound **1** was obtained as colorless block crystals. The positive ion peak in high resolution time-of-flight mass spectrometry (HRTOFMS) at *m/z* 385.2367 $[M + Na]^+$ was compatible with the molecular formula of $C_{22}H_{34}O_4$. The IR spectrum indicated absorptions of hydroxy (3334 $cm^{-1}$), ester carbonyl (1732 $cm^{-1}$) and olefinic groups (1642 $cm^{-1}$). Analysis of the $^{13}C$ NMR and DEPT data (Table 1) of **1** indicated 22 carbon resonances, corresponding to five methyls ($\delta_C$ 33.5, 23.1, 22.4, 21.8, and 21.4), five methylenes ($\delta_C$ 36.7, 35.8, 28.9, 25.1 and 19.7), one $sp^2$ methylene ($\delta_C$ 114.4), three oxygenated methines ($\delta_C$ 76.8, 72.7 and 68.2), two methines ($\delta_C$ 143.5 and 45.2), five quaternary carbons ($\delta_C$ 136.8, 127.5, 42.9, 39.9 and 33.4), and one ester carbonyl carbon ($\delta_C$ 170.7). The $^1H$ and $^{13}C$ NMR spectroscopic data (Table 1) displayed characteristic resonances of an isopimarane diterpene framework with a terminal vinyl group [$\delta_H/\delta_C$ 5.95 (1H, dd, $J$ = 17.6, 10.9 Hz, H-15)/143.5, 5.15 (1H, dd, $J$ = 10.9, 1.0 Hz, H-16 b)/114.4, and 5.10 (1H, dd, $J$ = 17.6, 1.0 Hz, H-16a)], three oxygenated methine groups [$\delta_H/\delta_C$ 5.60 (1H, br d, $J$ = 5.1 Hz, H-6)/68.2, 3.82 (1H, br s, H-1)/72.7 and 3.46 (1H, s, H-14)/76.8], four tertiary methyl groups [$\delta_H/\delta_C$ 1.31 (3H, s, H-20)/21.4, 0.99 (3H, s, H-19)/33.5, 0.99 (3H, s, H-18)/23.1 and 0.98 (3H, s, H-17)/22.4], and one acetoxy group [$\delta_H$ 2.00 (3H, s, 6-OAc)/21.8, $\delta_C$ 170.7]. These spectroscopic data were similar to the spectroscopic data of marginaol A previously isolated from the rhizomes of *K. marginata* collected from Phana district, Amnat Charoen Province (Chokchaisiri et al., 2020). The difference between these two compounds was that a double bond at C-8 (14) of marginaol A was replaced by a double bond at C-8 (9) in **1**, which was confirmed by heteronuclear multiple bond correlations (HMBCs) between $H_3$-20 ($\delta_H$ 1.31)/$H_2$ -12 ($\delta_H$ 1.46 and 1.84) and C-9 ($\delta_C$ 136.8) and between $H_2$ -7 ($\delta_H$ 1.99 and 2.75) and C-9 ($\delta_C$ 136.8)/C-8 ($\delta_C$ 127.5) (Fig. 2). Additionally, the presence of an acetoxy group at $\delta_H$ 2.00 (3H, s, C*H*$_3$OCO-6) was placed at C-6 due to the HMBC from H-6 with $CH_3O\underline{CO}$-6 ($\delta_C$ 170.7. The HMBCs from H-14 with C-8 ($\delta_C$ 127.5), C-9 ($\delta_C$ 136.8), C-15 ($\delta_C$ 143.5) and C-17 ($\delta_C$ 22.4) confirmed the location of the hydroxy group at C-14. The relative configuration of **1** was assigned by analysis of coupling constants and nuclear Overhauser effect (NOE) experiments, as shown in Fig. 3. The small vicinal coupling constant of H-1 that appeared as a broad singlet revealed its equatorial orientation, which was confirmed by the observation of an NOE effect between H-1/$CH_3$-18 and $CH_3$-20. The H-5 and H-6 protons were suggested to have *α*-orientations from NOE correlations between H-5/H-6, H-7α and H-19. The NOE correlations between H-14/H-7β and $H_3$-17 suggested *α*-orientations of the C-14 hydroxy group. The X-ray crystallographic pattern (Fig. 4) confirmed the structure of **1** as 1*α*,14*α*-dihydroxy-6*β*-acetoxyisopimara-8 (19),15-diene and named it marginaol G.

Compound **2**, colorless block crystals, gave the same molecular formula, $C_{22}H_{34}O_4$ (HRESITOFMS *m/z* 385.2360 $[M + Na]^+$) as **1**. The $^1H$ and $^{13}C$ NMR spectroscopic data (Table 1) of **2** were identical to the data of **1**, except that a carbinol proton at $\delta_H$ 3.43 (1H, s, H-14) was assigned as *α*-oriented. This finding was supported by the upfield shift of the $^{13}C$ NMR resonance of C-14 ($\delta_C$ 73.9) in **2** compared to $\delta_C$ 76.8 in **1**. The NOE difference experiment (Fig. 3) showed a correlation of H-14 with H-7α ($\delta_H$ 2.27). The structure of **2** was also verified by X-ray diffraction analysis (Fig. 4). Thus, the structure of **2** was assigned as 1*α*,14*β*-dihydroxy-6*β*-acetoxyisopimara-8 (19),15-diene and named marginaol H.

Compound **3** was a white amorphous solid. The molecular formula $C_{22}H_{34}O_3$ was determined from its HRESITOFMS data (*m/z* 369.2420 $[M + Na]^+$). The IR spectrum showed stretching bands of hydroxy (3499 $cm^{-1}$), ester carbonyl (1730 $cm^{-1}$), and olefinic groups (1641 $cm^{-1}$). The $^1H$ and $^{13}C$ NMR spectroscopic data (Table 1) of **3** were similar to the data of **1**, except for the disappearance of one oxygenated signal and the presence of methylene resonances at $\delta_H$ 1.41 and 1.65 ($H_2$ -6)/$\delta_C$ 17.9 (C-6). In addition, the resonance at $\delta_H$ 2.02 (3H, s) was

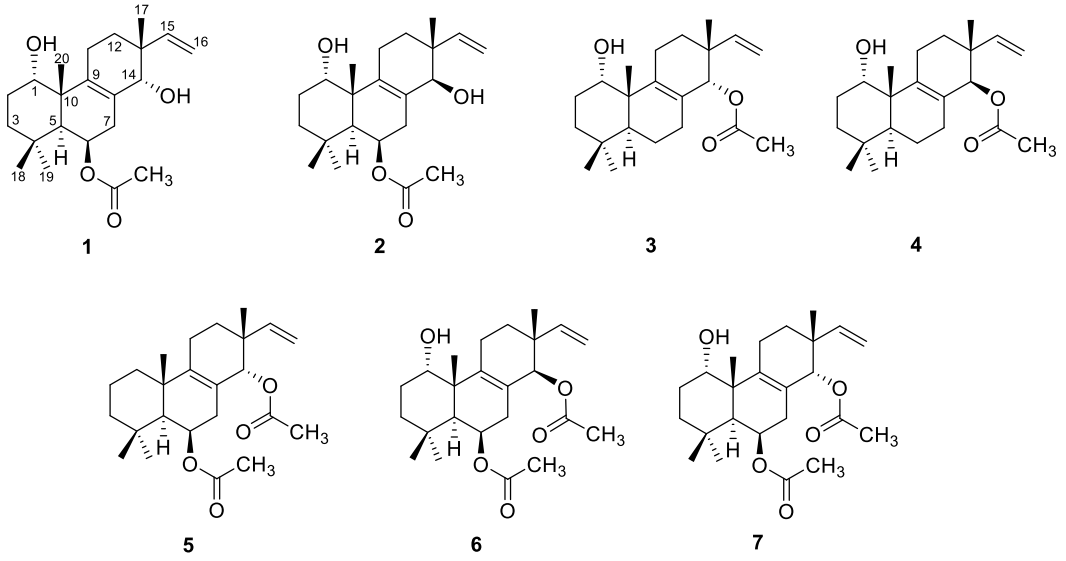


**Fig. 1.** Structures of marginaols G–M (**1**–**7**).

**Table 1**
$^{1}$H (400 MHz) and$^{13}$C NMR (100 MHz) data of compounds **1**–**4** ($CDCl_3$)[a].

| Position | 1 | | 2 | | 3 | | 4 | |
|---|---|---|---|---|---|---|---|---|
| | $\delta_C$ | $\delta_H$ (*J* in Hz) | $\delta_C$ | $\delta_H$ (*J* in Hz) | $\delta_C$ | $\delta_H$ (*J* in Hz) | $\delta_C$ | $\delta_H$ (*J* in Hz) |
| 1*β* | 72.7 | 3.82 (br s) | 72.7 | 3.76 (br s) | 71.2 | 3.84 (br s) | 71.2 | 3.81 (br s) |
| 2*α* | 25.1 | 1.56 (m) | 24.5 | 1.55 (m) | 24.9 | 1.56[b] | 24.6 | 1.59[b] |
| 2*β* | | 1.89 (m) | | 1.87 (m) | | 1.85[b] | | 1.83 (m) |
| 3*α* | 35.8 | 1.12 (dt, 10.4, 2.6) | 35.8 | 1.34 (m) | 34.3 | 1.18 (m) | 34.3 | 1.17 (m) |
| 3*β* | | 1.64 (m) | | 1.66 (m) | | 1.60[b] | | 1.65[b] |
| 4 | 33.4 | – | 33.3 | – | 32.9 | – | 32.9 | – |
| 5 | 45.2 | 1.75 (br s) | 45.1 | 1.74 (br s) | 44.1 | 1.51 (br s) | 44.1 | 1.48 (br s) |
| 6*α* | 68.2 | 5.60 (br d, 5.1) | 68.0 | 5.63 (br d, 5.1) | 17.9 | 1.41[b] | 18.1 | 1.37 (m) |
| 6*β* | | – | | – | | 1.65[b] | | 1.68 (m) |
| 7*α* | 36.7 | 2.75 (m) | 36.5 | 2.27 (m) | 28.9 | 2.07 (m) | 29.6 | 1.92 (m) |
| 7*β* | | 1.99[b] | | 2.52 (m) | | 1.81[b] | | 1.99 (m) |
| 8 | 127.5 | – | 128.9 | – | 129.0 | – | 129.0 | – |
| 9 | 136.8 | – | 137.5 | – | 139.4 | – | 140.4 | – |
| 10 | 42.9 | – | 43.0 | – | 43.3 | – | 43.1 | – |
| 11*α* | 19.7 | 2.07 (m) | 20.6 | 1.97 (m) | 20.1 | 2.03 (m) | 20.8 | 2.05[b] |
| 11*β* | | 2.21 (m) | | 2.15 (m) | | 2.26[b] | | 2.09 (m) |
| 12*α* | 28.9 | 1.46 (m) | 28.0 | 1.60 (m) | 30.8 | 1.48[b] | 29.3 | 1.49[b] |
| 12*β* | | 1.84 (m) | | 1.83 (m) | | 1.78[b] | | 1.56[b] |
| 13 | 39.9 | – | 39.8 | – | 39.2 | – | 39.1 | – |
| 14*α* | | – | 73.9 | 3.43 (s) | | – | 74.9 | 5.07 (s) |
| 14*β* | 76.8 | 3.46 (s) | | – | 78.6 | 5.14 (s) | | – |
| 15 | 143.5 | 5.95 (dd, 17.6, 10.9) | 144.4 | 5.71 (dd, 17.7, 11.0) | 142.4 | 5.92 (dd, 17.0, 10.7) | 143.2 | 5.71 (dd, 17.7, 11.0) |
| 16a | 114.4 | 5.10 (dd, 17.6, 1.0) | 112.2 | 4.92 (dd, 17.7, 1.2) | 113.0 | 5.02 (br d, 17.0) | 112.6 | 4.96 (br d, 17.7) |
| 16 b | | 5.15 (dd, 10.9, 1.0) | | 4.99 (dd, 11.0, 1.2) | | 5.02 (br d, 10.7) | | 4.99 (br d, 11.0) |
| 17 | 22.4 | 0.98 (s) | 23.9 | 1.04 (s) | 23.7 | 0.95 (s) | 23.6 | 0.92 (s) |
| 18 | 23.1 | 0.99 (s) | 23.1 | 0.98 (s) | 21.7 | 0.90 (s) | 21.7 | 0.84 (s) |
| 19 | 33.5 | 0.99 (s) | 33.5 | 0.99 (s) | 33.1 | 0.84 (s) | 33.1 | 0.91 (s) |
| 20 | 21.4 | 1.31 (s) | 21.1 | 1.31 (s) | 20.4 | 1.01 (s) | 20.2 | 1.01 (s) |
| 6-OCO$\underline{CH_3}$ | 21.8 | 2.00 (s) | 21.8 | 2.00 (s) | | | | |
| 6-O$\underline{CO}CH_3$ | 170.7 | – | 170.8 | – | | | | |
| 14-OCO$\underline{CH_3}$ | | | | | 21.1 | 2.02 (s) | 21.1 | 2.06 (s) |
| 14-O$\underline{CO}CH_3$ | | | | | 171.4 | – | 171.2 | – |

[a] Chemical shifts (δ) are given in ppm and J in Hz; assignments were based on distortion enhancement by polarization transfer (DEPT), heteronuclear multiple quantum correlation (HMQC), and heteronuclear multiple bond correlation (HMBC) experiments.
[b] Overlapping signal.

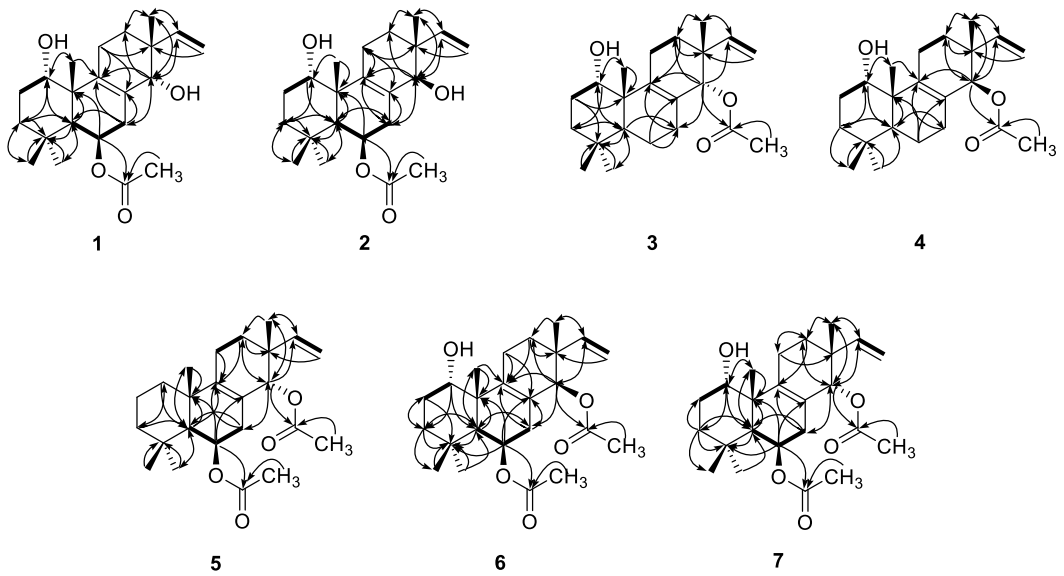


**Fig. 2.** The Correlated Spectroscopy (COSY) correlations and key HMBCs ($^{1}$H →$^{13}$C) of compounds **1**–**7**.

assigned to an acetoxy group, which could be located at C-14 from the HMBC of H-14 with $CH_3O\underline{CO}$-14 ($\delta_C$ 171.4) (Fig. 2). The α-orientations of the substituents at C-1 and C-14 were determined by analysis of their $^{1}$H NMR coupling constants and the NOE difference experiments compared to analogous values for compound **1** (Fig. 3). The very small coupling constants of H-1 (br s) indicated the equatorial orientation and were confirmed by the observation of the NOE effect between H-1/$H_3$-20. H-14 was suggested to be the *β*-orientation based on the NOE correlations between H-14/H-7*β* and $H_3$-17. Thus, the structure of **3** was assigned as 1*α*-hydroxy-14*α*-acetoxyisopimara-8 (19),15-diene and named marginaol I.

Compound **4** was isolated as a white amorphous solid and its

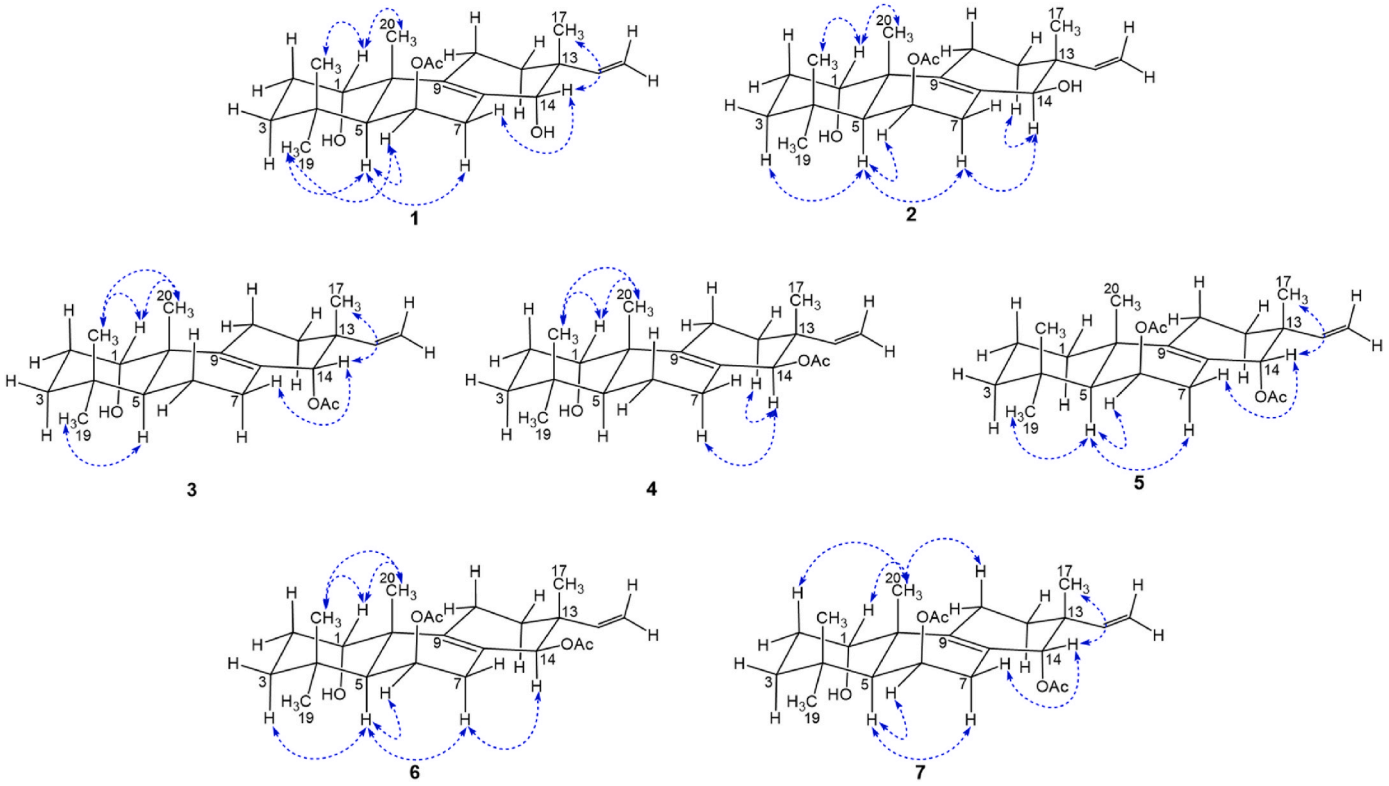

**Fig. 3.** Key NOE correlations and relative configuration of **1**–**7**. Arrows indicate identified NOE difference correlations.

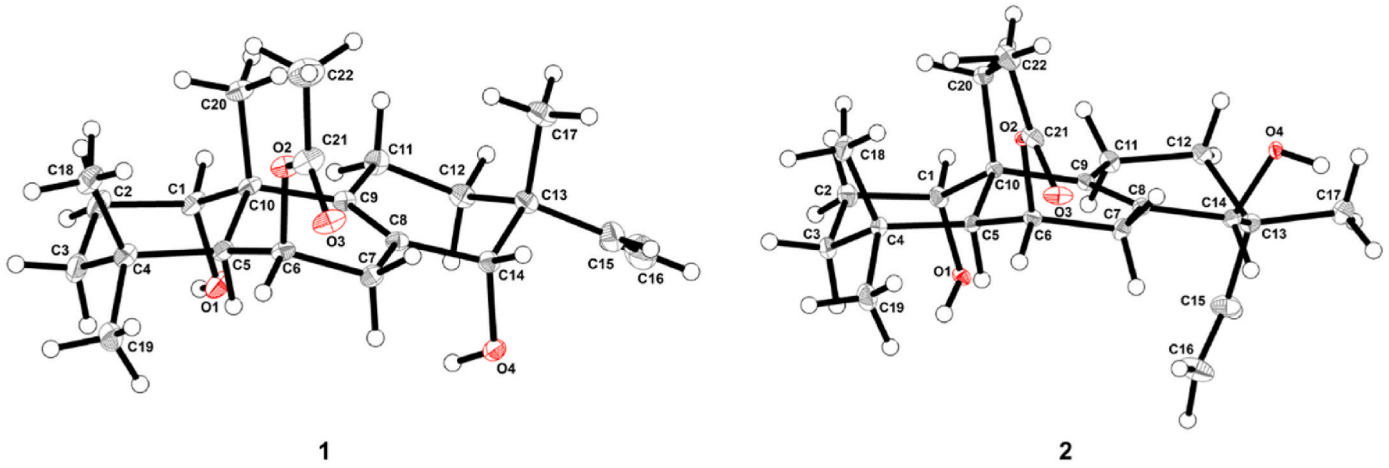

**Fig. 4.** X-ray crystallographic structures of **1** and **2**.

molecular formula $C_{22}H_{34}O_3$ was established by the HRESITOFMS ion peak at *m/z* 369.2416 $[M + Na]^+$. Its infrared (IR) spectra displayed the same pattern as the pattern of **3**. The NMR data (Table 1) of **4**, identical to marginaol I (**3**), indicated that **4** had the same structure framework as marginaol I. The difference was found that an acetoxy group at C-14 ($\delta_H$ 2.06) was fixed as $\beta$-orientation which was confirmed by the NOE effect between H-14/H-7α and H-11α (Fig. 3). Thus, the structure of **4** was assigned as 1$\alpha$-hydroxy-14$\beta$-acetoxyisopimara-8 (19),15-diene and named marginaol J.

Compound **5** was obtained as a white amorphous solid, with a characteristic molecular composition of $C_{24}H_{36}O_4$ (*m/z* 411.2528 $[M + Na]^+$) that was established by HRESITOFMS. The $^1H$ and $^{13}C$ NMR data (Table 2) of **5** closely resembled the data of **1**. The major difference in NMR data was found to be the absence of the oxymethine group at $\delta_C$ 72.7, which was assigned to C-1 in **1**; instead, **5** showed the presence of a methylene group ($\delta_C$ 39.1), which confirmed an HMBC to $H_3$-20 ($\delta_H$ 1.32). In addition, the oxymethine proton at $\delta_H$ 5.15 (H-14) showed HMBCs (Fig. 2) with $CH_3O\underline{CO}$-14 ($\delta_C$ 171.2), placing this additional acetyl group at C-14. Furthermore, the relative configurations were assigned based on the NOE difference experiment (Fig. 3), which showed the correlation between H-14/H-7$\beta$ and $H_3$-17, suggesting that the acetyl at C-14 is $\alpha$-oriented. Thus, the structure of **5** was assigned as 6$\beta$,14$\alpha$-diacetoxyisopimara-8 (19),15-diene and named marginaol K.

Compound **6**, obtained as a white amorphous solid, was analyzed for $C_{24}H_{36}O_5$ by a combination of HRESITOFMS (*m/z* 427.2475 $[M + Na]^+$) and $^{13}C$ NMR data. The $^1H$ and $^{13}C$ NMR spectroscopic data (Table 2) of **6** closely resembled the data of **2**, except for the presence of an acetoxy group at C-14 instead of the hydroxy moiety in **2**. The downfield shift of an oxymethine H-14 ($\delta_H$ 5.06) suggested the presence of an acetoxy moiety in **6**. Based on the HMBC correlations of H-14 with $CH_3O\underline{CO}$-14

**Table 2**
$^{1}$H (400 MHz) and$^{13}$C NMR (100 MHz) data of compounds **5**–**7** ($CDCl_3$)[a].

| Position | 5 | | 6 | | 7 | |
|---|---|---|---|---|---|---|
| | $\delta_C$ | $\delta_H$ (*J* in Hz) | $\delta_C$ | $\delta_H$ (*J* in Hz) | $\delta_C$ | $\delta_H$ (*J* in Hz) |
| 1*α* | 39.1 | 1.10[b] | | – | | – |
| 1*β* | | 1.73[b] | 72.7 | 3.77 (br s) | 72.6 | 3.80 (br s) |
| 2*α* | 20.0 | 1.54[b] | 24.4 | 1.59[b] | 24.6 | 1.58[b] |
| 2*β* | | 1.66[b] | | 1.85 (m) | | 1.86[b] |
| 3*α* | 43.1 | 1.15[b] | 35.7 | 1.12 (m) | 35.7 | 1.14[b] |
| 3*β* | | 1.35[b] | | 1.66[b] | | 1.66[b] |
| 4 | 33.3 | | 33.5 | – | 33.3 | – |
| 5 | 52.1 | 1.29 (br s) | 45.0 | 1.73 (br s) | 45.0 | 1.73 (br s) |
| 6*α* | 67.1 | 5.54 (br d, 5.7) | 67.8 | 5.57 (br d, 4.9) | 67.3 | 5.59 (br d, 5.2) |
| 6*β* | | – | | – | | – |
| 7*α* | 35.3 | 2.41 (br d, 18.7) | 35.9 | 2.22[b] | 35.0 | 2.41 (m) |
| 7*β* | | 1.83 (br d, 18.7) | | 2.01[b] | | 1.87[b] |
| 8 | 120.6 | | 125.4 | – | 125.9 | – |
| 9 | 142.7 | | 139.8 | – | 138.6 | – |
| 10 | 37.9 | | 43.1 | – | 43.2 | – |
| 11*α* | 20.3 | 2.01 (m) | 20.6 | 2.01[b] | 20.0 | 2.16 (m) |
| 11*β* | | 2.16 (m) | | 2.22[b] | 31.1 | |
| 12*α* | 31.2 | 1.54[b] | 29.1 | 1.53[b] | | 1.55[b] |
| 12*β* | | 1.71[b] | | 1.71[b] | 39.5 | 1.79[b] |
| 13 | 39.5 | | 39.2 | – | | – |
| 14*α* | | | 74.2 | 5.06 (s) | 78.3 | – |
| 14*β* | 78.2 | 5.15 (s) | | – | 141.8 | 5.21 (s) |
| 15 | 142.3 | 5.94 (dd, 17.4, 11.2) | 143.2 | 5.71 (dd, 17.8, 11.0) | 113.3 | 5.94 (dd, 18.0, 10.7) |
| 16a | 113.1 | 5.00 (br d, 17.4) | 112.7 | 4.95 (br d, 17.8) | | 5.04 (br d, 18.0) |
| 16 b | | 5.01 (br d, 11.2) | | 5.01 (br d, 11.0) | 24.3 | 5.05 (br d, 10.7) |
| 17 | 23.4 | 0.97 (s) | 23.6 | 0.92 (s) | 23.0 | 0.97 (s) |
| 18 | 23.2 | 0.97 (s) | 23.1 | 0.98 (s) | 33.5 | 0.98 (s) |
| 19 | 33.9 | 0.94 (s) | 33.3 | 0.98 (s) | 21.2 | 0.98 (s) |
| 20 | 21.1 | 1.32 (s) | 21.0 | 1.34 (s) | 21.7 | 1.32 (s) |
| 6-OCO$\underline{C}H_3$ | 21.7 | 2.00 (s) | 21.7 | 2.00 (s) | 170.6 | 1.99 (s) |
| 6-O$\underline{CO}CH_3$ | 170.7 | – | 170.6 | – | 20.9 | – |
| 14-OCO$\underline{C}H_3$ | 21.0 | 2.00 (s) | 20.0 | 2.03 (s) | 171.2 | 2.04 (s) |
| 14-O$\underline{CO}CH_3$ | 171.2 | – | 170.9 | – | 72.6 | – |

[a] Chemical shifts (δ) are given in ppm and J in Hz; assignments were based on DEPT, HMQC, and HMBC experiments.
[b] Overlapping signal.

($\delta_C$ 170.9), an acetoxy group was located at C-14. The NOE difference experiment (Fig. 3) showed that the correlation of **6** indicated that it had the same relative configuration as **2**. Thus, the structure of **6** was assigned as 1*α*-hydroxy-6*β*,14*β*-diacetoxyisopimara-8 (19),15-diene and named marginaol L.

Compound **7**, a white amorphous solid, gave the same molecular formula, $C_{24}H_{36}O_5$ (HRESITOFMS *m/z* 427.2466 $[M + Na]^+$), as **1**. The $^{1}$H and $^{13}$C NMR spectroscopic data (Table 2) of **7** were similar to the data of **1**, differing only in their substituents. Comparison of the spectroscopic data of **7** with the data of **1** indicated that the only difference was the presence of an additional acetoxy group at C-14. The HMBC cross-peak between C$\underline{H_3}$OCO-14 ($\delta_H$ 2.04) and C-14 ($\delta_C$ 78.3) and $CH_3O\underline{CO}$-14 ($\delta_C$ 171.2) placed this acetoxy moiety at C-14. The NOE difference experiments of **7** (Fig. 3) indicated that **7** had the same relative configuration as **1**. Thus, the structure of **7** was assigned as 1*α*-hydroxy-6*β*,14*α*-diacetoxyisopimara-8 (19),15-diene and named marginaol M.

The isolated isopimarane diterpenoids, **1**–**11**, were evaluated for their inhibition on of NO production in LPS-activated RAW264.7 cells (Table 3). All the compounds exhibited significant NO inhibitory activity. Compounds with an SI value greater than 20 were found to be the most effective at inhibiting NO secretion while being relatively less cytotoxic to cells. Among the compounds tested, compound **10** possessed the most potent NO inhibitory activity ($IC_{50}$ 4.5 ± 0.2 *μ*M; SI > 35.6), followed by compounds **3** ($IC_{50}$ 6.2 ± 2.0 *μ*M; SI > 25.8) and **1** ($IC_{50}$ 7.3 ± 1.1 μM; SI > 21.9). The inhibitory effect of Compound **10**, **3**, and **1** on NO was comparable to the inhibitory effect of the standard drug dexamethasone ($IC_{50}$ 4.7 ± 2.6 *μ*M; SI > 34.0). Compounds **2**, **4**, **6**–**9** and **11** are moderately active, with SI values ranging from >9.5 to 24.4, whereas compound **5** is particularly toxic to cells. Compounds **8** and **10** have been shown to suppress LPS-induced NO production in RAW264.7 cells with $IC_{50}$ values of 12.1 and 7.7 *μ*M, respectively, and their mechanism of action could be through suppression of iNOS mRNA expression (Tungcharoen et al., 2020). Furthermore, Compound 10 inhibited the expression of two additional inflammatory mediators, cyclooxygenase 2 (COX2) and TNF-α at the mRNA level (Tungcharoen et al., 2020).

**Table 3**
Inhibition of nitric oxide production and cytotoxicity of **1**–**10**.

| Compound | $IC_{50}$ (μM) | $CC_{50}$ (μM) | SI |
|---|---|---|---|
| **1** | 7.3 ± 1.1 | >160 | >21.9 |
| **2** | 5.5 ± 1.8 | 105.1 ± 26.2 | 19.1 |
| **3** | 6.2 ± 2.0 | >160 | >25.8 |
| **4** | 15.4 ± 4.5[b] | 153.8 ± 7.9 | 10.0 |
| **5** | 3.7 ± 0.1 | 29.0 ± 1.2 | 7.8 |
| **6** | 13.7 ± 3.2[b] | >160 | >11.7 |
| **7** | 9.5 ± 3.5[a] | 136.8 ± 23.2 | 14.4 |
| **8** | 8.8 ± 4.4 | >160 | >18.2 |
| **9** | 16.9 ± 6.8[b] | >160 | >9.5 |
| **10** | 4.5 ± 0.2 | >160 | >35.6 |
| **11** | 5.7 ± 1.9 | 138.9 ± 17.3 | 24.4 |
| Dexamethasone | 4.7 ± 2.6 | >160 | >34.0 |

$IC_{50}$, the half-maximal NO inhibitory concentration.
$CC_{50}$, the half-maximal cytotoxic concentration.
SI, selectivity index.
Dexamethasone was used as the reference drug.
Data represent the mean ± SD of three independent experiments in triplicate. [a], $p < 0.05$; [b], $p < 0.0001$ versus Dexamethasone.
The absence of a letter superscript indicates no significant difference from the effect of Dexamethazone.

## 3. Conclusions

In this study, seven previously undescribed isopimarane diterpenoids together with four known analogs were isolated from the rhizomes of *K. marginata*. The structures of these isolated compounds were characterized using related spectroscopic methods. In addition, the relative configurations of compounds **1** and **2** were ascertained by X-ray crystallographic analysis. Meanwhile, the anti-inflammatory effect of all compounds on LPS-stimulated NO production from RAW264.7 cells was evaluated. When compared to the standard dexamethasone, compound **10** has a comparable potency while remaining less cytotoxic to the host cells. This research contributes to the variety of diterpenoids derived from *Kaempferia* species and provides some basis for this medicinal plant in the alternate treatment of inflammatory illness.

## 4. Experimental

### 4.1. General experimental procedures

Melting points were determined with a BUCHI B-540 melting point apparatus and are uncorrected. Optical rotations were measured on a JASCO-1020 polarimeter. IR spectra were obtained using a PerkinElmer Fourier transform infrared (FT-IR) Spectrum BX spectrophotometer. $^{1}$H and $^{13}$C NMR spectra were recorded on a Bruker AVANCE 400 FT-NMR spectrometer, operating at 400 ($^{1}$H) and 100 ($^{13}$C) MHz. Chemical shifts (δ) were expressed in ppm with reference to the solvent signals. All isolated compounds were dissolved in chloroform-d ($CDCl_3$). Spectra were calibrated by assigning the residual solvent peaks to $\delta_H$ 7.24 and $\delta_C$ 77.0. Electrospray ionization (ESI)TOFMS data were measured with a Bruker microTOF mass spectrometer. Unless otherwise indicated, column chromatography was carried out using Merck silica gel 60 (<0.063 mm) and Pharmacia Sephadex LH-20. For TLC, Merck precoated silica gel 60 $F_{254}$ plates were used. Spots on TLC were detected under UV light and by spraying with anisaldehyde-$H_2SO_4$ reagent followed by heating.

### 4.2. Plant material

The rhizomes of *Kaempferia marginata* Carey ex Roscoe (Zingiberaceae) were collected from Phutthaisong district, Buri Ram province (15°32′54″N 103°1′30″E), Thailand, in January 2017 (dry season). A voucher specimen (Apichart Suksamrarn, No. 089) is deposited at the Faculty of Science, Ramkhamhaeng University.

### 4.3. Extraction and isolation

The air-dried rhizomes of *K. marginata* (5.0 kg) were milled and macerated successively with hexane, ethyl acetate (EtOAc) and methanol (MeOH) to yield the hexane (254.3 g), EtOAc (115.3 g) and MeOH (41.6 g) extracts, respectively, after evaporation of the solvents under reduced pressure.

The hexane extract (250.0 g) was fractionated by column chromatography (CC) (Merck silica gel 60, 0.063–0.200 mm, 520 g) using a gradient solvent system eluting with hexane followed by increasing polarity with EtOAc. The eluates were examined by thin layer chromatography (TLC), and eight combined fractions (H1–H8) were obtained. Fraction H1 (29.7 g) was subjected to CC using an isocratic solvent system of hexane−EtOAc (100:1) to give three subfractions (H1a−H1c). Subfraction H1c (15.8 g) was repeatedly recrystallized from hexane to afford compound **9** (2.43 g) as a white amorphous solid. Fraction H4 (38.8 g) was chromatographed eluting under isocratic conditions with hexane−EtOAc (90:10) to give five subfractions (H4a−H4e). Subfraction H4c (16.1 g) was recrystallized repeatedly from hexane to furnish compound **10** (7.66 g) as a white amorphous solid. Fraction H6 (37.14 g) was chromatographed eluting under isocratic conditions with $CH_2Cl_2$–MeOH (100:2) to produce four subfractions (H6a−H6d). Recrystallization of subfraction H6b by hexane−EtOAc (90:10) furnished compound **1** (933.5 mg). Subfraction H6c (3.81 g) was rechromatographed eluting with $CH_2Cl_2$–MeOH (100:0.5) to yield compound **2** (527.6 mg).

The EtOAc extract (110.0 g) was fractionated by CC (Merck silica gel 60, 0.063–0.200 mm, 250 g) using a gradient solvent system of hexane, hexane–EtOAc and EtOAc with increasing amounts of the more polar solvent. The eluates were examined by TLC, and ten combined fractions (E1−E10) were obtained. Fraction E2 (1.05 g) was subjected to column chromatography (twice) eluted under isocratic conditions with hexane−EtOAc (80:20) to give compound **3** (30.7 mg). Subfraction E4 (2.83 g) was subjected to CC using an isocratic solvent system of hexane−EtOAc (90:10) to furnish four subfractions (E4a−E4d). Subfraction E4c (359.3 mg) yielded compound **4** (34.9 mg) by using an isocratic solvent system of hexane−EtOAc (100:5). Fraction H4b (1.68 g) was further fractionated by CC using an isocratic solvent system of hexane−EtOAc (100:5) to afford compound **5** (5.9 mg). Fraction E6 (13.14 g) was chromatographed eluting under isocratic conditions with hexane−EtOAc (90:10) to yield six subfractions (E6a−E6f). Subfraction E6b (6.80 g) was separated on a Sephadex LH-20 column eluting with $CH_2Cl_2$–MeOH (20:80) followed by silica gel CC eluting with $CH_2Cl_2$–MeOH (100:1) to give compounds **6** (17.9 mg) and **7** (42.8 mg). Subfraction E6d (401.2 mg) was separated on a Sephadex LH-20 column eluting with $CH_2Cl_2$–MeOH (20:80) to afford compound **11** (25.3 mg) as a white amorphous solid. Fraction E7 (10.66 g) was chromatographed eluting under isocratic conditions with hexane−EtOAc (100:25) to give five subfractions (E7a−E7e). Subfraction E7b (843.9 mg) was repeatedly recrystallized from hexane−EtOAc (100:5) to afford compound **8** (129.3 mg) as a white amorphous solid.

#### 4.3.1. Marginaol G (1)

Colorless block crystal; mp: 163–164 °C; $[\alpha]_D^{24}$ –17.8 (*c* 0.97, $CHCl_3$); IR: $\nu_{max}$ 3334, 2933, 1732, 1642, 1457, 1379, 1275, 1011, 907 cm$^{-1}$; $^{1}$H and $^{13}$C NMR data, see Table 1; HRTOFMS (ESI$^+$): *m/z* 385.2367 [M + Na]$^+$ (calcd for $C_{22}H_{34}O_4Na$, 385.2349).

#### 4.3.2. Marginaol H (2)

Colorless block crystal; mp: 161–162 °C; $[\alpha]_D^{24}$ 64.5 (*c* 0.81, $CHCl_3$); IR: $\nu_{max}$ 3500, 2983, 1714, 1641, 1464, 1365, 1260, 1219, 1027, 915 cm$^{-1}$; $^{1}$H and $^{13}$C NMR data, see Table 1; HRTOFMS (ESI$^+$): *m/z* 385.2367 [M + Na]$^+$ (calcd for $C_{22}H_{34}O_4Na$, 385.2349).

#### 4.3.3. Marginaol I (3)

White amorphous solid; mp: 129–130 °C; $[\alpha]_D^{24}$ –15.1 (*c* 0.42, $CHCl_3$); IR: $\nu_{max}$ 3499, 2931, 1730, 1641, 1454, 1370, 1275, 1010, 909 cm$^{-1}$; $^{1}$H and $^{13}$C NMR data, see Table 1; HRTOFMS (ESI$^+$): *m/z* 369.2420 [M + Na]$^+$ (calcd for $C_{22}H_{34}O_3Na$, 369.2400).

#### 4.3.4. Marginaol J (4)

White amorphous solid: 123–124 °C; 113.9 (*c* 1.54, $CHCl_3$); IR: $\nu_{max}$ 3464, 2934, 1731, 1668, 1460, 1370, 1235, 1014, 910 cm$^{-1}$; $^{1}$H and $^{13}$C NMR data, see Table 1; HRTOFMS (ESI$^+$): *m/z* 369.2416 [M + Na]$^+$ (calcd for $C_{22}H_{34}O_3Na$, 369.2400).

#### 4.3.5. Marginaol K (5)

White amorphous solid; 121–122 °C $[\alpha]_D^{24}$ –65.7 (*c* 0.68, $CHCl_3$); IR: $\nu_{max}$ 2929, 1734, 1639, 1461, 1367, 1229, 1027, 969 cm$^{-1}$; $^{1}$H and $^{13}$C NMR data, see Table 2; HRTOFMS (ESI$^+$): *m/z* 411.2528 [M + Na]$^+$ (calcd for $C_{24}H_{36}O_4Na$, 411.2505).

#### 4.3.6. Marginaol L (6)

White amorphous solid; 131–132 °C; $[\alpha]_D^{24}$ 117.0 (*c* 1.47, $CHCl_3$); IR: $\nu_{max}$ 3516, 2928, 1724, 1704, 1461, 1375, 1258, 1020, 909 cm$^{-1}$; $^{1}$H and $^{13}$C NMR data, see Table 2; HRTOFMS (ESI$^+$): *m/z* 427.2475 [M + Na]$^+$ (calcd for $C_{24}H_{36}O_5Na$, 427.2454).

#### 4.3.7. Marginaol M (7)

White amorphous solid; 134–135 °C; $[\alpha]_D^{24}$ –16.3 (*c* 0.91, $CHCl_3$); IR: $\nu_{max}$ 3498, 2930, 1730, 1710, 1453, 1369, 1237, 1020, 907 $cm^{-1}$; $^1H$ and $^{13}C$ NMR data, see Table 2; HRTOFMS ($ESI^+$): *m/z* 427.2466 $[M + Na]^+$ (calcd for $C_{24}H_{36}O_5Na$, 427.2479).

### 4.4. X-ray crystallographic analysis

The single crystal data were collected using a Rigaku XtalLab SuperNova diffractometer equipped with a microfocus sealed X-ray tube of Mo *K*α radiation (λ = 0.71073 Å) and a direct photon counting HyPix3000 detector. The datasets were processed by CrysAlisPro the program (Rigaku Oxford Diffraction, 2018), and the multiscan absorption corrections were applied. The crystal structures were solved by intrinsic phasing methods within the SHELXT program and refined on F2 by the full-matrix least-squares technique using the SHELXL program (Sheldrick, 2015) via the Olex 2 interface (Dolomanov et al., 2009). All hydrogen atoms were generated from mixed geometrically and difference Fourier maps. The crystallographic data of structures **1** (CCDC no. 2113132) and **2** (CCDC no. 2113133) have been deposited at the Cambridge Crystallographic Data Centre (CCDC; http://www.ccdc.cam.ac.uk/structures/).

#### 4.4.1. Crystallographic data for marginaol G (1)

$C_{22}H_{34}O_4$, M = 362.49, colorless block crystal, orthorhombic, space group $P2_12_12_1$, *a* = 15.2874 (5) Å, *b* = 16.5090 (5) Å, *c* = 17.1295 (7) Å, V = 4323.1 (2) $Å^3$, *Z* = 8, $D_{calc}$ = 1.138 g/$cm^3$, T = 293 (2) K, *F* (000) = 1616 and $\mu$ = 0.078 $mm^{-1}$. A total of 24,764 reflections (8699 unique, *R*int = 0.0501) were collected with index ranges of $-19 \leq h \leq 18$, $-19 \leq k \leq 20$, and $-21 \leq l \leq 18$. The final stage converged to $R_1 = 0.0528$ ($wR_2 = 0.1186$) for observed reflections [with $I > 2\sigma(I)$], 521 variable parameters, 9 restraints and goodness of fit = 0.959.

#### 4.4.2. Crystallographic data for marginaol H (2)

$C_{22}H_{34}O_4$, M = 362.49, colorless block crystal, orthorhombic, space group $P2_12_12_1$, *a* = 7.4669 (2) Å, *b* = 13.1667 (6) Å, *c* = 20.2081 (10) Å, V = 1986.75 (14) $Å^3$, *Z* = 4, $D_{calc}$ = 1.212 g/$cm^3$, T = 293 (2) K, *F* (000) = 792 and $\mu$ = 0.081 $mm^{-1}$. A total of 11,469 reflections (4011 unique, *R*int = 0.0543) were collected with index ranges of $-8 \leq h \leq 9$, $-16 \leq k \leq 16$, and $-19 \leq l \leq 25$. The final stage converged to $R_1 = 0.0515$ ($wR_2 = 0.1050$) for observed reflections [with $I > 2\sigma(I)$], 258 variable parameters, 1 restraints and goodness of fit = 1.002.

### 4.5. Nitric oxide inhibitory activity

RAW264.7 cells ($3 \times 10^5$ cells/$cm^2$) were seeded into 96-well plates and grown for 24 h. Cells were preincubated with various concentrations of compounds **1**–**11** (0–160 $\mu$M) and dexamethasone as a standard drug for 1 h following 10 ng/mL LPS stimulation. After 24 h of incubation, 75 $\mu$L of supernatant was collected and mixed with 65 $\mu$L of distilled water and 10 $\mu$L of Griess reagent (1% sulfanilamide and 0.1% naphthylethylene in 2.5% phosphoric acid solution) in a 96-well plate according to the described method (Griess, 1879). A microplate reader (Thermo Fisher, USA). was used to measure absorbance at 540 nm after 30 min of incubation at room temperature. A $NaNO_2$ serial dilution standard curve was used to determine the nitrite concentration. The half-maximal NO inhibitory concentration ($IC_{50}$) of the compounds and dexamethasone was determined from a dose-response curve using GraphPad Prism 6 (GraphPad Software Inc, CA, USA). Data were obtained from three independent experiments in triplicate.

### 4.6. Cytotoxicity assays

RAW 264.7 cells were grown in a 96-well plate at a density of $3 \times 10^5$ cells/$cm^2$ for 24 h. Cells were treated with the compounds at various concentrations (0–160 μM). After 24 h of treatment, the cells were incubated with 0.5 mg/mL MTT solution for an additional 3 h before the solution was removed. The formazan crystal products were dissolved in 200 μL of dimethyl sulfoxide (DMSO) in each well. A microplate reader was used to measure the absorbance of the formazan solution at a wavelength of 560 nm. Cell viability was calculated using the following equation: [(*A* treated sample/*A*n untreated sample) × 100]. GraphPad Prism 6 (GraphPad Software Inc, CA, USA) was used to calculate the half-maximal cytotoxic concentration ($CC_{50}$) of the compounds and dexamethasone. Three independent experiments in triplicate yielded the results.

### 4.7. Selectivity index (SI)

The selectivity of the compounds in inhibiting NO secretion over cytotoxicity was determined using SI values. A high SI value suggests a high level of NO secretion inhibition with minimal cytotoxicity. The SI values were determined by dividing the $CC_{50}$ value by the $IC_{50}$ value.

### 4.8. Statistical analysis

All experimental data are expressed as the mean ± standard deviation (SD) of in three independent experiments. The significant differences in the $IC_{50}$ values among the tested compounds were determined using one-way analysis of variance (ANOVA) followed by Dunnett's multiple comparison test in GraphPad Prism V9.3.0 (GraphPad Software, CA, USA). A significant difference was considered at $p < 0.05$.

## Declaration of competing interest

The authors declare that they have no known competing financial interests or personal relationships that could have appeared to influence the work reported in this paper.

## Acknowledgments

This work was supported by the Thailand Science Research and Innovation (TSRI) fund and University of Phayao (Grant No. FF65-RIM048 and FF64-UoE033). Partial support from the Center of Excellence for Innovation in Chemistry (PERCH-CIC) are gratefully acknowledged.

## Appendix A. Supplementary data

Supplementary data to this article can be found online at https://doi.org/10.1016/j.phytochem.2022.113225.

## References

Chokchaisiri, R., Chaichompoo, W., Chunglok, W., Cheenpracha, S., Ganranoo, L., Phutthawong, N., Bureekaew, S., Suksamrarn, A., 2020. Isopimarane diterpenoids from the rhizomes of *Kaempferia marginata* and their potential anti-inflammatory activities. J. Nat. Prod. 83, 14–19. https://doi.org/10.1021/acs.jnatprod.9b00307.

Chokchaisiri, R., Chaichompoo, W., Pabuprapap, W., Sukcharoen, O., Tocharus, J., Ganranoo, L., Bureekaew, S., Sangvichien, E., Suksamrarn, A., 2021. Biotransformation of 1α,11α-dihydroxyisopimara-8(14),15-diene by *Cunninghamella echinulata* NRRL 1386 and their neuroprotective activity. Bioorg. Chem. 110, 104799. https://doi.org/10.1016/j.bioorg.2021.104799.

Devi, K.P., Malar, D.S., Nabavi, S.F., Sureda, A., Xiao, J., Nabavi, S.M., Daglia, M., 2015. Kaempferol and inflammation: from chemistry to medicine. Pharmacol. Res. 99, 1–10. https://doi.org/10.1016/j.phrs.2015.05.002.

Diaz-Jimenez, D., Kolb, J.P., Cidlowski, J.A., 2021. Glucocorticoids as regulators of macrophage-mediated tissue homeostasis. Front. Immunol. 12, 1–14. https://doi.org/10.3389/fimmu.2021.669891.

Do, K.M., Kodama, T., Shin, M.K., Nu, L.H.T., Nguyen, H.M., Dang, S.V., Shiokawa, K.I., Hayakawa, Y., Morita, H., 2022. Marginols A–H, unprecedented pimarane diterpenoids from *Kaempferia marginata* and their NO inhibitory activities. Phytochemistry 196, 113109. https://doi.org/10.1016/j.phytochem.2022.113109.

Dolomanov, O.V., Bourhis, L.J., Gildea, R.J., Howard, J.A.K., Puschmann, H., 2009. OLEX2: a complete structure solution, refinement and analysis program. J. Appl. Cryst. 42, 339–341. https://doi.org/10.1107/S0021889808042726.

Efferth, T., Oesch, F., 2021. The immunosuppressive activity of artemisinin-type drugs towards inflammatory and autoimmune diseases. Med. Res. Rev. 1–39. https://doi.org/10.1002/med.21842.

Fallahi, F., Borran, S., Ashrafizadeh, M., Zarrabi, A., Pourhanifeh, M.H., Khaksary Mahabady, M., Sahebkar, A., Mirzaei, H., 2021. Curcumin and inflammatory bowel diseases: from in vitro studies to clinical trials. Mol. Immunol. 130, 20–30. https://doi.org/10.1016/j.molimm.2020.11.016.

Griess, J.P., 1879. Bemerkungen zu der Abhandlung der HH. Weselsky und Benedikt "Ueber einige Azoverbindungen. J. Griess. Ber. Deutsch. Chem. Ges. 12, 426–428. https://doi.org/10.1002/cber.187901201117.

He, F.Q., Qiu, B.Y., Zhang, X.H., Li, T.K., Xie, Q., Cui, D.J., Huang, X.L., Gan, H.T., 2011. Tetrandrine attenuates spatial memory impairment and hippocampal neuroinflammation via inhibiting NF-κB activation in a rat model of Alzheimer's disease induced by amyloid-β(1-42). Brain Res. 1384, 89–96. https://doi.org/10.1016/j.brainres.2011.01.103.

Hu, Q., Lyon, C.J., Fletcher, J.K., Tang, W., Wan, M., Hu, T.Y., 2021. Extracellular vesicle activities regulating macrophage and tissue-mediated injury and repair responses. Acta Pharm. Sin. B11, 1493–1512. https://doi.org/10.1016/j.apsb.2020.12.014.

Kaewkroek, K., Wattanapiromsakul, C., Kongsaeree, P., Tewtrakul, S., 2013. Nitric oxide and tumor necrosis factor-alpha inhibitory substances from the rhizomes of *Kaempferia marginata*. Nat. Prod. Commun. 8, 1205–1208. https://doi.org/10.1177/1934578X1300800904.

Madaka, F., Tewtrakul, S., 2011. Anti-allergic activity of some selected plants in the genus *Boesenbergia* and *Kaempferia*. Songklanakarin J. Sci. Technol. 33, 301–304.

Moussa, C., Hebron, M., Huang, X., Ahn, J., Rissman, R.A., Aisen, P.S., Turner, R.S., 2017. Resveratrol regulates neuro-inflammation and induces adaptive immunity in Alzheimer's disease. J. Neuroinflammation 14, 1–10. https://doi.org/10.1186/s12974-016-0779-0.

Obaid, M., Udden, S.M.N., Deb, P., Shihabeddin, N., Zaki, M.H., Mandal, S.S., 2018. LncRNA HOTAIR regulates lipopolysaccharide-induced cytokine expression and inflammatory response in macrophages. Sci. Rep. 8, 1–18. https://doi.org/10.1038/s41598-018-33722-2.

Prawat, U., Tuntiwachwuttikul, P., Taylor, W.C., Engelhardt, L.M., Skelton, B.W., White, A.H., 1993. Diterpenes from a *Kaempferia* species. Phytochemistry 32, 991–997. https://doi.org/10.1016/0031-9422(93)85242-J.

Rigaku Oxford Diffraction, 2018. CrysAlisPRO Software System. Rigaku Corporation, Oxford, UK versions 1.171.39.46.

Ross, E.A., Devitt, A., Johnson, J.R., 2021. Macrophages: the good, the bad, and the gluttony. Front. Immunol. 12, 1–22. https://doi.org/10.3389/fimmu.2021.708186.

Seong, K.J., Lee, H.G., Kook, M.S., Ko, H.M., Jung, J.Y., Kim, W.J., 2016. Epigallocatechin-3- gallate rescues LPS impaired adult hippocampal neurogenesis through suppressing the TLR4 NF-κB signaling pathway in mice. Korean J. Physiol. Pharmacol. 20, 41–51. https://doi.org/10.4196/kjpp.2016.20.1.41.

Sheldrick, G.M., 2015. Crystal structure refinement with SHELXL. Acta Cryst. C Struct. Chem. C71, 3–8. https://doi.org/10.1107/S2053229614024218.

Tan, W.S.D., Liao, W., Zhou, S., Wong, W.S.F., 2017. Is there a future for andrographolide to be an anti-inflammatory drug? Deciphering its major mechanisms of action. Biochem. Pharmacol. 139, 71–81. https://doi.org/10.1016/j.bcp.2017.03.024.

Thongnest, S., Mahidol, C., Sutthivaiyakit, S., Ruchirawat, S., 2005. Oxygenated pimarane diterpenes from *Kaempferia marginata*. J. Nat. Prod. 68, 1632–1636. https://doi.org/10.1021/np050186l.

Tungcharoen, P., Wattanapiromsakul, C., Tansakul, P., Nakamura, S., Matsuda, H., Tewtrakul, S., 2020. Anti-inflammatory effect of isopimarane diterpenoids from *Kaempferia galanga*. Phyther. Res. 34, 612–623. https://doi.org/10.1002/ptr.6549.

Win, N.N., Ito, T., Aimaiti, S., Kodama, T., Imagawa, H., Ngwe, H., Asakawa, Y., Abe, I., Morita, H., 2015. Kaempulchraols I-O: new isopimarane diterpenoids from *Kaempferia pulchra* rhizomes collected in Myanmar and their antiproliferative activity. Tetrahedron 71, 4707–4713. https://doi.org/10.1016/j.tet.2015.05.075.